# Submillimeter-Scale MEMS-Based Jumping Microbots

Luca Garlati, Jaren Hubal, and Scott Wade

***Abstract*—Creating small-scale mobile robots is a challenge that has been the topic of much research. Scaling down mechanics and designs introduces many challenges, including manufacturing, small-scale physics, and control. Past terrestrial robots on the sub-millimeter scale have been able to locomote in limited capacity with electrically and thermally induced moving parts; however, jumping robots have not been adequately explored. This report discusses a bio-inspired MEMS robot that can jump similar to a springtail arthropod. Our process uses a thermal bimorph actuator to generate and store up to 126 pJ of elastic energy, which is released by a latch once sufficient energy is stored. When the energy is released, the bimorph actuator launches the robot into the air with 1.25m/s of initial velocity, propelling it to heights of 200x the device length.**

## I. Introduction

Miniaturized robots are of great interest to researchers due to the many potential novel applications they might have. Currently, millimeter and submillimeter-scale robots have potential applications in medicine, manufacturing, and remote sensing. However, they may have niche uses beyond these which may not emerge until the technology develops further, much like semiconductor research begat the computer.

At microscopic scales, robot locomotion can present a serious challenge. Researchers have explored several modes of locomotion, with varying degrees of success. Achieving efficient walking and crawling gaits can prove quite challenging, and often such gaits have strong dependence on the texture of the terrain being navigated. Thus, researchers have begun to thoroughly investigate jumping in microrobotics.

Previous jumping microbots have been produced, but only on a millimeter scale and with heavy actuation mechanisms. Bergbreiter, Pister, and Greenspun explored a microrobot architecture that used an inchworm drive to load a flexural spring or elastomer, but only achieved limited jumping performance at a multi-millimeter or centimeter sale [1]–[3].

Other recent research has produced mobile microrobots at a submillimeter scale. However, actuation and control present a large challenge with submillimeter-scale microrobots. Some works have used conductive surfaces to convey energy to their robots, which constrains the microrobots to artificial environments [4]. Other works have used lasers to actuate and energize microrobots. Miskin et al. successfully actuated a 40μmx40μm aquatic microrobot using a laser to energize photovoltaic cells [5]. Similarly, Han et al. actuated their submillimeter-scale terrestrial robot by heating shape memory actuators using a laser [6].

Another shortcoming of previous microbots is their lack of flexibility: their designs are limited to accomplishing a specific task. In contrast, we aimed to design a microbot that can be implemented alongside other devices.

We propose a novel submillimeter-scale jumping mechanism that is thermally actuated. By using a thermal bimorph actuator, our mechanism is able to achieve high jumping performance via untethered actuation methods, allowing for integration with other submillimeter-scale devices to create higher complexity microrobots.

## II. Device Design

Jumping devices generally have a way to store energy and a way to release that energy as a short burst of kinetic energy. Our design accomplishes these two tasks using a thermal bimorph actuator and a passive latch. The thermal bimorph actuator, constrained by the latch, generates and stores energy as elastic stress. Once the actuator is heated enough, the force that it exerts on the passive latch causes the latch to slip or break, allowing the bimorph to quickly move out of plane towards the ground. The bimorph contacts the ground, translating its potential energy to kinetic energy, and forcing the robot to jump.

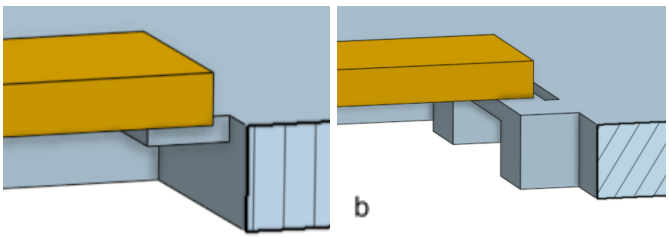


**Fig. 1.** Two types of latch mechanisms explored.

We considered two potential latch mechanisms to release the loaded actuator. The first is a cantilever beam, shown in Figure 1a. In this configuration, the actuating beam would apply a load near the end of the latch until the latch bends enough for the actuator to slip off. The second mechanism is a bar attached loosely to the sides, shown in Figure 1b. This bar would break off when sufficient force is applied. We selected the second mechanism to simplify modeling.

### *A. Mechanical Analysis*

A mechanical analysis was performed to model the system. These equations were used to determine

parameters such as materials, actuation temperature, and geometry, as well as to estimate performance.

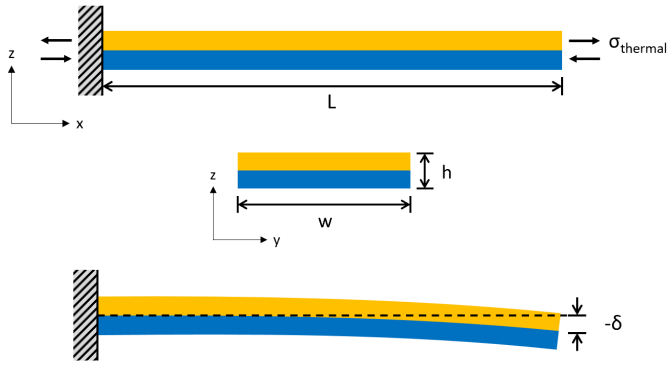


**Fig. 2.** Model of unconstrained bimorph actuator.

The full system is composed of two parts: a bimorph actuator and a latch. The bimorph actuator is shown in Figure 2, unconstrained by the latch. The bimorph bends due to different thermal stresses in the top and bottom sections of the beam. When the temperature of the beam changes, the change in bending angle with respect to the change in length can be modeled with (1).

$$\frac{d\theta}{dx} = \frac{\alpha_{bottom}\left(T_{bottom}-T_0\right)-\alpha_{top}\left(T_{top}-T_0\right)}{h} \quad (1)$$

In (1), $\alpha_{top}$ and $\alpha_{bottom}$ are the thermal coefficients of the top and bottom materials of the bimorph respectively, $T_{top}$ and $T_{bottom}$ are the final temperatures after the beam has been heated, $T_0$ is the initial temperature, and $h$ is the total height of the beam. Equation (1) can be integrated twice to derive the maximum deflection, $\delta$, in the beam after a temperature change. The maximum deflection, calculated with (2), occurs at the free end of the cantilever beam. In (2), $L$ is the length of the beam, and by convention an upward deflection is positive.

$$\delta = \frac{L^2}{2} * \frac{d\theta}{dx} \quad (2)$$


**Fig. 3.** Model of the system.

When the latch is added, the bimorph actuator can be modeled as a beam with one fixed end and one roller end representing the latch, as shown in Figure 3. $F_B$ is the force that the latch applies to the beam to hold it in place as it charges up. The latch breaks, releasing the beam, when $F_B$ is greater than the latch can handle. A relationship for $F_B$ is given in (3).

$$F_B = \frac{-3\delta E_{top} I}{L^3} \quad (3)$$

$E_{top}$ is the elastic modulus for the top material of the bimorph and $I$, given in (4), is the moment of inertia of the bimorph.

$$I = \left(\frac{1}{12}wh_{top}^{\ 3} + A_{top}\left(\bar{z}_{top} - \bar{z}\right)^2\right) + \left(\frac{1}{12}nw\left(h - h_{top}\right)^3 + A_{bottom}\left(\bar{z}_{bottom} - \bar{z}\right)^2\right) \quad (4)$$

In (4), $w$ is the width of the beam, $h_{top}$ and $h_{bottom}$ are the heights of the top and bottom portions of the beam respectively, $A_{top}$ and $A_{bottom}$ are the cross-sectional areas, $n$ is the modular ratio given in (5), and $\bar{z}$ is the distance from the bottom of the beam to the centroid, derived in (6), (7), and (8), where $\bar{z}_{top}$ and $\bar{z}_{bottom}$ are the centroids of the top and bottom sections of the bimorph respectively.

$$n = \frac{E_{bottom}}{E_{top}} \quad (5)$$

$$\bar{z}_{top} = h - \frac{h_{top}}{2} \quad (6)$$

$$\bar{z}_{bottom} = \frac{h-h_{top}}{2} \quad (7)$$

$$\bar{z} = \frac{A_{top}\bar{z}_{top}+A_{bottom}\bar{z}_{bottom}}{A_{top}+A_{bottom}} \quad (8)$$

The thermal moment, $M_{thermal}$ and reaction moment, $M_A$, can be found using (9) and (10).

$$M_{thermal} = E_{top} I \frac{d\theta}{dx} \quad (9)$$

$$M_A = M_{thermal} + F_B L \quad (10)$$

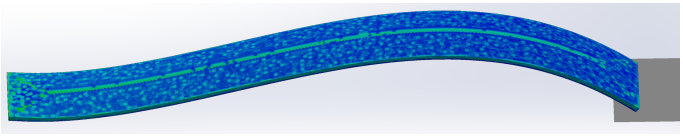

**Fig. 4.** Bimorph actuator when charged, displacement amplified 10x. High stress areas shown in green.

Figure 4 shows the shape of the bimorph actuator in its charged state. At full charge, $F_B$ is maximized. The elastic potential energy (U) stored in the actuator can be computed with (11).

$$U = \frac{3M_A^2 L - 3M_A F_B L^2 + F_B^2 L^3}{6E_{top} I} \quad (11)$$

Using conservation of energy, height that the device jumps can be calculated using (12).

$$H = \frac{U}{mg} \quad (12)$$

*B. Material Selection and Performance*

For the top beam, we selected aluminum with a height of 2 microns. For the bottom beam and latch, we selected silicon dioxide with a height of 1 micron. We

designed the actuator beam to be 50 microns wide and 400 microns long, and the latch to be 10 microns wide and 50 microns long.

Plugging in dimensions and material properties to the equations in section A, we found that this latch can withstand 16.7 N of force, and so the charged actuator stores 0.126 nJ of energy. This device would jump a maximum height of 7.9 cm, or 198 times the device length.

We simulated the actuator beam using these dimensions to validate our analysis and measure stress across the beam. Figure 3 shows the distribution of stress within the bimorph, which remains below the yield strength of the materials used.

## III. Fabrication

The fabrication process is designed to be as simple as possible to keep in line with our design philosophy. To achieve this, we included a couple uncommon process steps: oxide growing via pattern, and an aluminum etching mask. The former is necessary to ensure a near flat surface before depositing the bimorph. Without it, the performance of the device would be unpredictable. As for the aluminum mask, this reduces the fabrication process steps, and reduces the amount of material necessary for fabrication. We begin with a bare substrate, shown in Figure 5.


**Fig. 5.** Bare Substrate.

We then deposit a layer of silicon, illustrated in red in Figure 6, followed by poly silicon, depicted in green.

**Fig. 6.** Substrate with initial sacrificial layers.

Next, we anisotropically dry etch the polysilicon, shown in Figure 7, using the STS 320 RIE, $CF_4$+$O_2$, 100W @ 13.56MHz, 60mTorr process established by Willilams et al. [8]. This gives us access to the silicon below in our desired pattern.

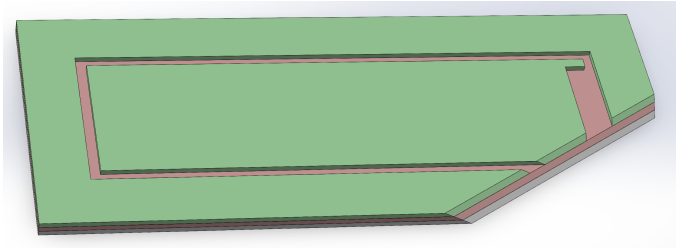

**Fig. 7.** Etch into sacrificial polysilicon.

Now, we need to deposit the latch oxide layer. Because slight variations can cause the bimorph to behave unexpectedly, it is critical that this layer of oxide be as flush with the poly as possible. One approach is to deposit a full layer of oxide and planarize the surface. However, that is slow, expensive, and complicated. As such, we propose growing the oxide layer up from the silicon, as its growth is well documented and controllable. This first oxide is shown in blue in Figure 8.

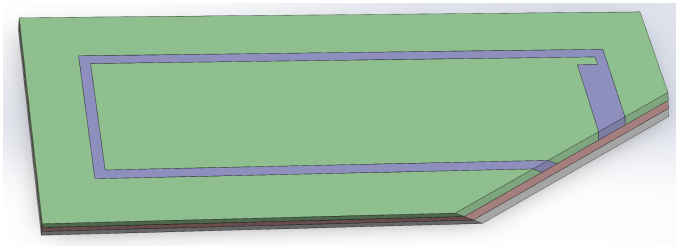

**Fig. 8.** Structure after oxide growth.

Next, we deposit a layer of a second oxide to form the bottom layer of the bimorph, depicted in pink in Figure 9.

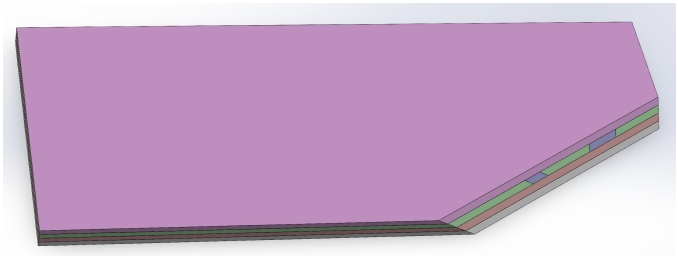

**Fig. 9.** Second oxide layer deposition.

Here, we evaporate aluminum onto the secondary oxide in our desired pattern, illustrated in cyan in Figure 10. This aluminum will then be used as the etching pattern for the oxide. Qu et al. demonstrated the viability of this process in their thermal bimorph paper [7]. This reduces the number of process steps and material necessary for fabrication compared to a traditional full layer deposition and etching process.

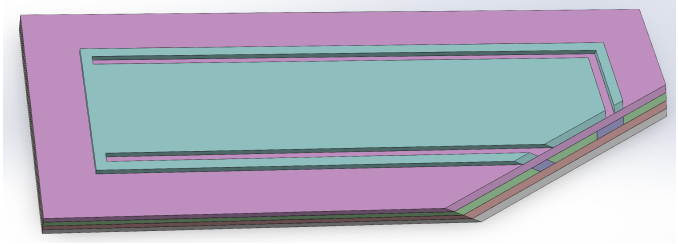

**Fig. 10.** structure after aluminum evaporation.

We then anisotropically etch the second oxide layer using the same process used on the green poly layer, as shown in Figure 11.

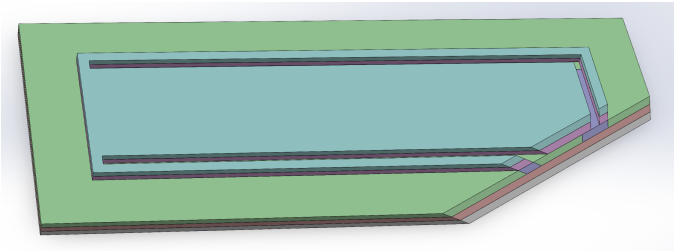

**Fig. 11.** Structure after anisotropic oxide etch.

Finally, we isotropically etch the poly and silicon below with uncharged $XeF_2$ gas, which does not attack either of the oxides, but rapidly etches the poly and silicon [8]. Further, because $XeF_2$ is a gas and not a liquid, it does not displace the assembly or cause issues with liquid adhesion once released. This step is shown in Figure 12.

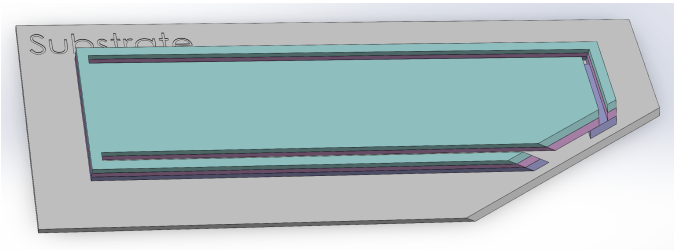


**Fig. 12.** Completed and freed structure.

Unlike other jumping robots, our device is ready to be activated immediately after release. No wire bonding or other secondary processes are necessary.

## IV. Results & Discussion

We present the first mechanism for enabling jumping locomotion in submillimeter-scale microrobots. Our proposed design achieves comparable performance to jumping robots many times its size, as shown in Table 1, while being the first jumping device in its length and weight class.

However, there were some limitations to our current design. The energy that can be stored in a single bimorph actuator is relatively low compared to previous works. Thus, while the standalone jumping performance of this jumper is acceptable, the payloads that the jumper can carry must be of a similarly small scale.

Another factor that should be considered before application of this jumping mechanism is the adhesion between the two layers of the bimorph actuator. Since a lot of bending stress is accumulated in the bimorph, delamination is a real concern. Future work should examine whether this phenomenon will interfere with the jumping mechanism.

In spite of these limitations, the presented jumping mechanism has demonstrated several features that enable the creation of new submillimeter-scale robots. The mechanism is very small, lightweight, and easy to integrate into larger robots. In addition, it can be easily actuated using a variety of thermal mechanisms, such as environmental heating, joule heating and laser heating. In the future, this mechanism could enable researchers to develop a new class of submillimeter-scale microrobot.

TABLE I
Comparison of Proposed Device With Previous Works

| | **This Work** | **G&P 2018 [1]** | **Yun. et al. 2023 [9]** | **Koh. et al. 2013 [10]** |
|---|---|---|---|---|
| Mass (ug) | 1.62E-04 | 43000 | 12000 | 34000 |
| Length (mm) | 0.40 | 6.4 | 3.4 | 20 |
| Jump Height (mm) | 79.35 | 1 | 295.8 | 300 |
| Jump Velocity (m/s) | 1.25 | N/A | 1 | 2.7 |

## References


[1] J. Greenspun and K. S. J. Pister, “FIRST LEAPS OF AN ELECTROSTATIC INCHWORM MOTOR-DRIVEN JUMPING MICROROBOT,” 2018 Solid-State, Actuators, and Microsystems Workshop Technical Digest, May 2018, doi: 10.31438/trf.hh2018.45.

[2] S. Bergbreiter and K. S. J. Pister, “Design of an autonomous jumping microrobot,” Proceedings, Apr. 2007, doi: 10.1109/robot.2007.363827.

[3] A. P. Gerratt and S. Bergbreiter, “Incorporating compliant elastomers for jumping locomotion in microrobots,” Smart Materials and Structures, vol. 22, no. 1, p. 014010, Dec. 2012, doi: 10.1088/0964-1726/22/1/014010.

[4] M. Z. Miskin et al., “Electronically integrated, mass-manufactured, microscopic robots,” Nature, vol. 584, no. 7822, pp. 557–561, Aug. 2020, doi: 10.1038/s41586-020-2626-9.

[5] M. Han et al., “Submillimeter-scale multimaterial terrestrial robots,” Science Robotics, vol. 7, no. 66, May 2022, doi: 10.1126/scirobotics.abn0602.

[6] B. R. Donald, C. G. Levey, C. D. McGray, I. Paprotny, and D. Rus, “An untethered, electrostatic, globally controllable MEMS Micro-Robot,” Journal of Microelectromechanical Systems, vol. 15, no. 1, pp. 1–15, Feb. 2006, doi: 10.1109/jmems.2005.863697.

[7] A. Jain, H. Qu, S. Todd, and H. Xie, “A thermal bimorph micromirror with large bi-directional and vertical actuation,” Sensors and Actuators A: Physical, vol. 122, no. 1, pp. 9–15, Jul. 2005, doi: 10.1016/j.sna.2005.02.001.

[8] K. R. Williams, K. Gupta, and M. Wasilik, “Etch rates for micromachining processing-part II,” Journal of Microelectromechanical Systems, vol. 12, no. 6, pp. 761–778, Dec. 2003, doi: 10.1109/jmems.2003.820936.

[9] R. Yun, Z. Liu, J. Leng, J. Huang, Y. Cui, X. Yan, and M. Qi, “A 3.4-millimeter flea-sized robot with powerful jumping and fast crawling locomotion,” IEEE Robotics and Automation Letters, vol. 8, no. 5, pp. 2868–2873, 2023.

[10] J.-S. Koh, S.-p. Jung, R. J. Wood, and K.-J. Cho, “A jumping robotic insect based on a torque reversal catapult mechanism,” in 2013 IEEE/RSJ International Conference on Intelligent Robots and Systems, pp. 3796–3801, IEEE, 2013.